Quantum State Tomography of an Itinerant Squeezed Microwave Field

F. Mallet,[1] M. A. Castellanos-Beltran,[1,2] H. S. Ku,[1,2] S. Glancy,[3] E. Knill,[3] K. D. Irwin,[3] G. C. Hilton,[3] L. R. Vale,[3] and K. W. Lehnert[1,2,*]

[1]*JILA, National Institute of Standards and Technology and the University of Colorado, Boulder, Colorado 80309, USA*
[2]*Department of Physics, University of Colorado, Boulder, Colorado 80309, USA*
[3]*National Institute of Standards and Technology, Boulder, Colorado 80305, USA*

(Received 3 December 2010; published 1 June 2011)

We perform state tomography of an itinerant squeezed state of the microwave field prepared by a Josephson parametric amplifier (JPA). We use a second JPA as a preamplifier to improve the quantum efficiency of the field quadrature measurement from 2% to 36% ± 4%. Without correcting for the detection inefficiency we observe a minimum quadrature variance which is 68^{+9}_{-7}% of the variance of the vacuum. We reconstruct the state's density matrix by a maximum likelihood method and infer that the squeezed state has a minimum variance less than 40% of the vacuum, with uncertainty mostly caused by calibration systematics.

DOI: 10.1103/PhysRevLett.106.220502 PACS numbers: 03.67.Bg, 03.65.Wj, 42.50.Dv, 42.50.Lc

Fundamental quantum optics experiments at microwave frequencies have been recently performed with superconducting qubits or Rydberg atoms inside high-quality microwave cavities. Examples include the reconstruction of the Wigner functions of Fock states from one [1] to a few photons and coherent superpositions of few photons [2–4]. States such as these, which are manifestly nonclassical light states, are crucial for quantum-information processing, because they can be used to generate entanglement. However, in the cited experiments, these states are confined in cavities. Therefore, distributing entanglement to separate parties, as required in quantum communication protocols, remains challenging for microwave implementations. In contrast to the discrete Fock state approach, continuous variables quantum-information (CVQI) strategy uses another type of nonclassical states, the squeezed states, which are readily created in itinerant modes. These states exhibit reduced noise, below the vacuum fluctuations, in one of their quadrature components and amplified noise in the other one. They are also easily generated at optical frequencies in the itinerant output modes of parametric amplifiers made of optically nonlinear crystals. At optical frequencies, CVQI has progressed rapidly from the initial creation of squeezed states [5] and tomographic reconstruction [6–8] of those states to teleportation [9,10] and quantum error correction [11,12].

At microwave frequencies, the field is less advanced. The generation of microwave squeezed states using the nonlinear electrical response of superconducting Josephson junctions has been reported [13], with inferred squeezing down to 10% of vacuum variance [14]. Such states can be powerful tools for quantum-information processing and communication because microwaves and superconducting qubits can mimic useful light-atom interactions, as demonstrated in [15]. Furthermore, these devices are made of compact and integrable electrical circuits, with much promise for building complex quantum-information processors. The lack of an efficient quadrature measurement (QM) for itinerant modes has slowed the advancement of CVQI. However, as demonstrated recently in [16], it is possible with a Josephson parametric amplifier (JPA) to realize an efficient single QM.

In this Letter, we report the tomography of an itinerant squeezed microwave field. We demonstrate that our JPA-based measurement scheme has a quantum efficiency 20 times greater than a QM employing state-of-art semiconductor amplifiers. We infer the quantum state prepared by maximum likelihood tomography, correcting for inefficiency in our QM. We discuss the achieved degree of squeezing, from the perspective of generating entanglement on chip.

Homodyne tomography is a standard experimental tool to infer the quantum state of a single mode of light. It was proposed in [17] and pioneered on a squeezed optical field in [6]. Its principle is depicted in Fig. 1. A homodyne detection apparatus measures the value of the quadrature X_θ, where θ is set by adjusting the phase of the local oscillator. The probability density function $\mathrm{pr}(X_\theta)$ for measuring a particular value of X_θ is the marginal density function of the Wigner function, i.e., $\mathrm{pr}(X_\theta) = \int dX_{\theta+\pi/2} W(X_\theta, X_{\theta+\pi/2})$, as shown in Fig. 1(b). Thus, by performing measurements of X_θ on many identical copies of the state and varying θ, the "hidden" quantum object can be seen from different angles and its state inferred. Losses and other Gaussian noise sources in the homodyne detector can be modeled with the insertion of a fictitious beam splitter of transmissivity η, as shown in Fig. 1(a). In such a case, the measured $\mathrm{pr}(X_\theta)$ are no longer the projections of the desired Wigner function W, but of a smoother distribution which is the convolution of W with a Gaussian Wigner function [18]. However, methods like

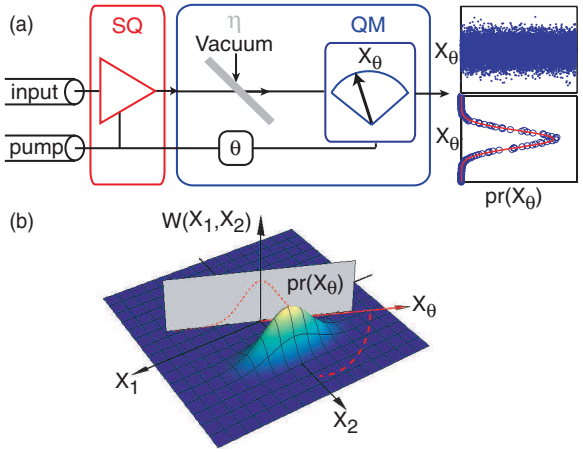

FIG. 1 (color). Principle of the experiment. (a) (Left) The squeezer (SQ, in red) prepares a squeezed state whose quadrature distributions are measured for different phases θ with an efficiency η. (Right) Simulated measurement results for 20 000 realizations of creating the squeezed state and measuring it at a single θ. The top graph shows the measured quadrature value versus realization number. The bottom plot is a histogram (blue circles) and Gaussian probability distribution pr(X_θ) (red curve) of this random process. (b) Graphical interpretation. The probability distribution pr(X_θ) is simply the projection of the Wigner function.

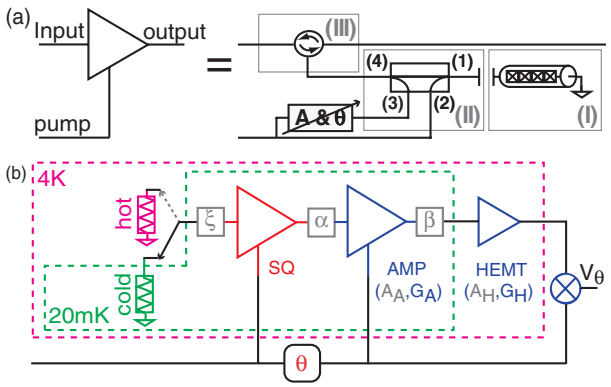

FIG. 2 (color). (a) To implement a SQ or AMP at microwaves, three microwave components are required: (i) a JPA, (ii) a directional coupler, and (iii) a circulator. Taking port (1) of the directional coupler as reference, (2) is the weakly coupled port, (3) the isolated port, and (4) the direct port. Port (2) is used to pump the JPA. Port (3) is used to apply a cancellation tone (adjusted with a room temperature attenuator and phase shifter) that nulls the pump and displaces the output of the JPA back to the origin of the phase space. (b) Schematic of the experiment. In this figure, all the microwave components and cables are considered lossless; their imperfections are absorbed into the experimentally determined total transmissivities ξ, α, and β.

maximum likelihood quantum state tomography can be used to deconvolve the effect of inefficiency [19].

At optical frequencies, $\eta \geq 90\%$ is routinely obtained using a pair of balanced photodiodes [19]. Such detectors are not available for microwaves and until recently the best setup was a chain of phase-insensitive amplifiers followed by a mixer, or two such chains in parallel [20–22]. In such a case, noise A_n greater than $1/2$ (the vacuum variance) must be added to the QM [23]. This noise can be modeled as an effective efficiency by the relation $\eta = 1/(1 + 2A_n)$ [24], so the QM efficiency using phase-insensitive amplifiers is limited to 50%. State-of-the-art microwave amplifiers, high-electron-mobility transistors (HEMTs), have $A_n \approx 10$–20. In practice, the unavoidable losses present in a microwave experiment typically result in $\eta \approx 2\%$. However, as demonstrated in [16], inserting a JPA used as a single quadrature preamplifier before the HEMT increases the experimentally achieved η by a factor of approximately 20.

To perform a high-quality reconstruction of the Wigner function of a squeezed microwave state we operate two JPAs in series, as shown in Fig. 2(b). The first JPA, referred to as the squeezer (SQ), prepares the squeezed state. The second JPA, referred to as the preamplifier (AMP), amplifies the quadrature of the squeezed state determined by the phase difference θ between the AMP and the SQ pump tones. We vary θ by applying to the two cavities pump tones slightly detuned from one another. The SQ stage is pumped at 7.45 GHz, while the AMP stage is pumped at 100 kHz higher frequency, therefore sweeping θ through 2π every 10 μs.

Our implementation of a SQ or an AMP at microwaves, as shown in Fig. 2(a), requires three elements: (i) a JPA used in reflection, (ii) a directional coupler, and (iii) a circulator. As described in [14], the JPAs are nonlinear resonant cavities built from coplanar waveguides whose central conductor has been replaced by a series of many Josephson junctions. The Josephson junctions' nonlinearity causes the cavity's phase velocity to be intensity dependent. Therefore, when the cavity is pumped it becomes a phase-sensitive amplifier for input modes whose frequencies lie within the bandwidth of the JPA centered on the pump frequency. Such microwave modes incident on the JPA are reflected and exit the cavity with one quadrature amplified and the other squeezed, depending on their phase relative to the pump's phase. A directional coupler is used to add the pump tone to the incident signal and remove the pump tone from the reflected signal. Finally, the incident and reflected modes are separated into different cables using a circulator.

Following Fig. 2(b), in the limit of large HEMT power gain G_H, our quantum efficiency can be cast as

$$\eta = \frac{\alpha}{2 + 2A_A - \alpha + [2A_H - (1 - \beta)]/G_A\beta}, \quad (1)$$

where A_A (A_H) is the AMP (HEMT) added noise, α (β) is the fraction of power transmitted by the microwave circuitry between the SQ and the AMP (the AMP and the HEMT), and G_A is the power gain of the AMP stage.

A detailed description of how we calibrate each of these parameters is in the supplemental information [25]. Briefly, we inject different amounts of thermal noise into the amplifier chain while operating each JPA either as an amplifier (on) or as a noiseless element with unit gain (off). We then infer the added noise and loss of the elements by observing the variation in the noise at the output of the measurement chain. The thermal noise is varied by connecting the input of the SQ through a switch to either a "hot load" (50Ω microwave termination at 4.1 K) or a "cold load" (at 20 mK). Although the tomography is only performed with the "cold load," both are required for calibration. We obtain $A_A = 0.25 \pm 0.06$, $A_H = 17.3 \pm 0.1$, $\alpha = 68 \pm 2\%$, and $\beta = 74 \pm 5\%$. However, as the switch is operated at the 4.1 K stage and is slightly lossy, the state presented at the input of the SQ with the "cold load" is not pure quantum vacuum, but a low occupancy thermal state with average photon number $\bar{n} \simeq 0.15 \pm 0.15$. One quadrature of the resulting squeezed state is then amplified at the AMP stage with sufficient gain $G_A = 180$ such that the noise in the amplified quadrature exceeds A_H for any θ. From Eq. (1), we obtained an overall quantum efficiency of $36 \pm 4\%$, which can be compared to $\eta \approx 2\%$ without the AMP stage.

In this experiment our uncertainty in η and $\bar{n}$ creates a systematic source of error. We thus perform our data analysis under three assumptions: (1) high efficiency ($\eta = 0.40$) and high mean photon number ($\bar{n} = 0.30$), (2) best estimate for both efficiency ($\eta = 0.36$) and mean photon number ($\bar{n} = 0.15$), and (3) low efficiency ($\eta = 0.33$) and low mean photon number ($\bar{n} = 0$). These three cases give us "pessimistic," "best-guess," and "optimistic" analyses, in terms of the purity of the squeezed state estimated by the tomography. Using a lower estimate for η and $\bar{n}$ as inputs to the tomography algorithm causes it to return a more pure, more squeezed, and therefore a more "optimistic" estimate of the squeezed state. Associated with each of these three cases, we also have statistical uncertainty, so the given error bounds cover an interval that includes both uncertainties around the "best-guess" estimate. They are reported in the form X^{+U}_{-L}, where X is the statistical mean using the best-guess calibration and L and U are, respectively, the lower and upper bounds of the 1 standard deviation uncertainty in the pessimistic and optimistic cases.

We must also calibrate the QM to convert the measured voltage noise into units of noise quanta. In optical homodyne tomography, this is usually done by inserting the vacuum and observing the quadrature noise. Analogously, we insert the weak thermal state with mean photons $\bar{n}$ (by simply turning the SQ stage off) and measure voltages proportional to quadrature values at many θ, as shown (in blue) in Fig. 3. As expected, this voltage noise is θ independent, with a variance $\Delta V^2_{\mathrm{SQ,off}} = 3.2 \times 10^{-5}$ mV^2. Under the convention that vacuum has variance 1/2

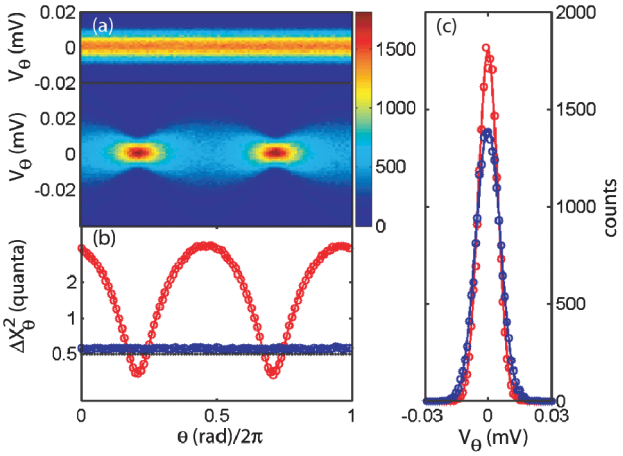

FIG. 3 (color). (a) Density plot of number of occurrences in a 1 μV bin size of the amplified quadrature voltage V_θ versus $\theta/2\pi$, with the SQ pump off (top) and on (bottom). (b) In particular, histograms of V_θ at the maximum of squeezing: data (○) and Gaussian fit (continuous lines) for the SQ pump off (blue) and on (red). (c) Noise variance ΔX^2_θ in quanta units on a log scale versus $\theta/2\pi$ for the SQ pump on (red) and off (blue). The (black) line indicates our estimate of the vacuum noise level under the "best-guess" calibration.

in unitless quadrature space (or in units of "quanta"), we calibrate this voltage variance to $\Delta X^2_{\mathrm{SQ,off}} = (1-\eta)/2 + \eta(1/2 + \bar{n}) = 0.55^{+0.07}_{-0.05}$ quanta. Therefore, the desired conversion factor $\Delta X^2_{\mathrm{SQ,off}}/\Delta V^2_{\mathrm{SQ,off}} = 1.71^{+0.20}_{-0.17} \times 10^4$ quanta/mV^2 is used to rescale the variances in Fig. 3(c).

In Fig. 3(a), we show QM data of the squeezed state. With SQ on (red) we observe the characteristic phase dependent noise for a squeezed state. At the phase for which the variance is minimum, we show the histogram of quadrature measurements in Fig. 3(b). The SQ off histogram is clearly wider than the SQ on histogram, demonstrating our ability to observe squeezing directly at the output of our measurement chain. In Fig. 3(c) we plot the variance of the QM with SQ on and off as a function of θ, expressed in units of quanta, clearly showing squeezing below the vacuum level. Without correcting for η, we observe a minimum quadrature variance which is $\Delta X^2_{\mathrm{SQ,min}} = 68^{+9}_{-7}\%$ of the vacuum variance.

To infer the quantum state created by the squeezer, correcting for loss during the QM, we used maximum likelihood quantum state tomography [26]. For each of the three calibration cases, we performed 35 reconstructions using independent subsets each containing 10 000 QMs of the total measured data. We estimated statistical uncertainty from the spread of properties (such as fidelity or minimum variance) of the set of 35 reconstructions. The statistical uncertainty was significantly lower than the systematic uncertainty. In Fig. 4 we show the Wigner function of the "best-guess" reconstructed state ρ. The pure squeezed vacuum state $|\psi\rangle$ that has the highest

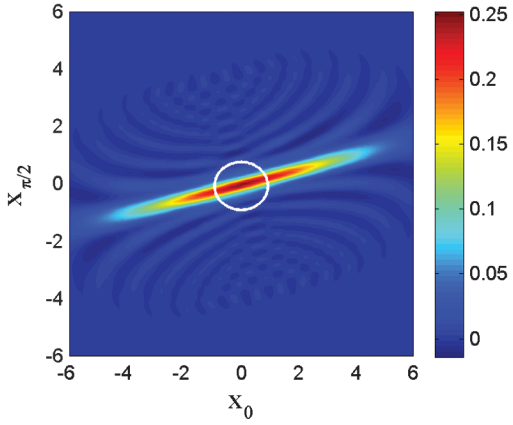

FIG. 4 (color). Mean of 35 reconstructions of the Wigner function of the state exiting the SQ, inferred by maximum likelihood under the "best-guess" assumption, in quanta units. The faint pattern of ripples extending from the origin is caused by truncation at 30 photons of the density matrix used to represent the state. The white circle at the origin shows the full width at half maximum of the vacuum state.

fidelity with ρ has minimum quadrature variance $6.0^{+1.4}_{-1.1}\%$ of the vacuum variance, and that maximum fidelity is $F = \langle\psi|\rho|\psi\rangle = 0.81^{+0.16}_{-0.17}$. As explained in the supplemental information [25], the minimum variance of ρ is biased by an amount comparable to our systematic uncertainty, so we infer the loss corrected minimum variance $\Delta x^2_{\mathrm{SQ,min}}$ directly from the observed minimum variance as $\Delta x^2_{\mathrm{SQ,min}} = (1/\eta)[\Delta X^2_{\mathrm{SQ,min}} - (1-\eta)/2]$. We find $\Delta x^2_{\mathrm{SQ,min}} = 12^{+30}_{-12}\%$ of the vacuum variance. For comparison, the most highly squeezed optical state ever made has a variance of only 7% of the vacuum variance [27].

Producing squeezed states of itinerant modes allows the generation of distributable entanglement by sending two copies of a squeezed vacuum state through the two input ports of a balanced beam splitter. The coherent information [28] is one useful way to characterize the entanglement between the two output modes. The asymptotic number of maximally entangled qubit pairs (ebits) that can be distilled per copy of the noisy entangled state, by using local operations and one-way classical communication, is at least as large as the coherent information [29]. Given two copies of ρ, one could make two entangled modes with $2.5^{+1.0}_{-0.4}$ ebits of coherent information.

In conclusion, we have reconstructed the Wigner function of an itinerant squeezed microwave field generated at the output of a Josephson parametric amplifier. Using a second JPA as a preamplifier has increased the quantum efficiency of the microwave homodyne detection from approximately 2% to 36%. The level of squeezing is primarily limited by noise added to the squeezed state by the JPA. Improving the performance of the JPAs (as both squeezers and phase-sensitive amplifiers) will require more detailed investigation of the source of this noise. We used maximum likelihood quantum state tomography to deconvolve the QM inefficiency in order to precisely characterize the state generated. This is an important step toward generating easily distributable microwave entanglement on chip.

The authors acknowledge support from the DARPA/MTO QuEST program.

Note added.—A different method was recently used to obtain a similar state reconstruction [30].

*konrad.lehnert@jila.colorado.edu

[1] A. A. Houck *et al.*, Nature (London) **449**, 328 (2007).
[2] S. Deléglise *et al.*, Nature (London) **455**, 510 (2008).
[3] M. Hofheinz *et al.*, Nature (London) **454**, 310 (2008).
[4] M. Hofheinz *et al.*, Nature (London) **459**, 546 (2009).
[5] R. E. Slusher *et al.*, Phys. Rev. Lett. **55**, 2409 (1985).
[6] D. T. Smithey *et al.*, Phys. Rev. Lett. **70**, 1244 (1993).
[7] S. Schiller *et al.*, Phys. Rev. Lett. **77**, 2933 (1996).
[8] G. Breitenbach, S. Schiller, and J. Mlynek, Nature (London) **387**, 471 (1997).
[9] A. Furusawa *et al.*, Science **282**, 706 (1998).
[10] H. Yonezawa, S. L. Braunstein, and A. Furusawa, Phys. Rev. Lett. **99**, 110503 (2007).
[11] T. Aoki *et al.*, Nature Phys. **5**, 541 (2009).
[12] M. Lassen *et al.*, Nat. Photon. **4**, 700 (2010).
[13] B. Yurke *et al.*, Phys. Rev. Lett. **60**, 764 (1988).
[14] M. A. Castellanos-Beltran *et al.*, Nature Phys. **4**, 929 (2008).
[15] A. Wallraff *et al.*, Nature (London) **431**, 162 (2004).
[16] J. D. Teufel *et al.*, Nature Nanotech. **4**, 820 (2009).
[17] K. Vogel and H. Risken, Phys. Rev. A **40**, 2847 (1989).
[18] U. Leonhardt and H. Paul, Phys. Rev. A **48**, 4598 (1993).
[19] A. I. Lvovsky and M. G. Raymer, Rev. Mod. Phys. **81**, 299 (2009).
[20] E. P. Menzel *et al.*, Phys. Rev. Lett. **105**, 100401 (2010).
[21] M. Mariantoni *et al.*, Phys. Rev. Lett. **105**, 133601 (2010).
[22] D. Bozyigit *et al.*, Nature Phys. **7**, 154 (2010).
[23] C. M. Caves, Phys. Rev. D **26**, 1817 (1982).
[24] U. Leonhardt and H. Paul, Phys. Rev. Lett. **72**, 4086 (1994).
[25] See supplemental material at http://link.aps.org/supplemental/10.1103/PhysRevLett.106.220502 for a discussion of data acquisition, calibration, and maximum likelihood analysis.
[26] Z. Hradil *et al.*, in *Quantum State Estimation* (Springer, Berlin, 2004), pp. 59–112.
[27] M. Mehmet *et al.*, Phys. Rev. A **81**, 013814 (2010).
[28] B. Schumacher and M. A. Nielsen, Phys. Rev. A **54**, 2629 (1996).
[29] I. Devetak and A. Winter, Proc. R. Soc. A **461**, 207 (2005).
[30] C. Eichler *et al.*, following Letter, Phys. Rev. Lett. **106**, 220503 (2011).